affect the characteristics of the various wings at vanishing or small flap deflection angles. The asymmetric leading edge had a lower aerodynamic efficiency (Fig. 6) than the symmetric one (Fig. 5), whereas the concave leading edge increased the aerodynamic efficiency at positive angles of attack (Fig. 7).

The difference between the aerodynamic characteristics of the flapped wings at negative and positive angles of attack, as mentioned before, and Rao's suggestion that leeward deflections could improve the wing performance, led to the investigation of the inverted flapped wing, because the flap hinges were not designed for large upward, or leeward, deflections. Although the wing was not designed to operate in an upside-down position, it was assumed, that as the leading-edge shape affect was small, the trends of leeward-deflection effects could be at least qualitatively evaluated. Generally speaking, the results of the leeward flap deflection were antisymmetrical to those of the downward deflection that were described above. α_{0L} became negative which caused the lift at positive angles of attack to increase. The drag increased significantly with all the flaps at angles of attack above 4 deg. The maximum aerodynamic efficiency was obtained when the flaps were not deflected. The aerodynamic efficiency of the configurations with windward deflections was higher than those with the leeward flap deflections. However, this result must be qualified because the generic wing is asymmetrical, and has different efficiencies at negative and positive angles of attack.

References

[1]Polhamus, E. C., "Prediction of Vortex Characteristics by a Leading-Edge Suction Analogy," *Journal of Aircraft*, Vol. 8, No. 4, 1971, pp. 193–197.

[2]Lamar, J. E., and Campbell, J. F., "Vortex Flaps—Advanced Control Devices for Supercruise Fighters," *Aerospace America*, Jan. 1984, pp. 95–99.

[3]Lee, C. S., "Experimental Studies of a Delta Wing with Leading-Edge Flaps," Joint Inst. for Aeronautics and Acoustics, Stanford Univ., JIAA TR-76, Stanford, CA, Aug. 1987.

[4]Oh, S., Tavella, D., and Roberts, L., "Theoretical Studies on Flapped Delta Wings," Joint Inst. for Aeronautics and Acoustics, Stanford Univ., JIAA TR-85, Stanford, CA, Aug. 1988.

[5]Hoffer, K. D., Rao, D. M., and Frassenelli, M. C., "Low-Speed Aerodynamics of Apex Fences on a Tailess Delta Configuration," AIAA Paper 86-1838, June 1986.

[6]Rao, D. M., and Johnson, T. D., Jr., "Subsonic Pitch-Up Alleviation on a 74 Degree Delta Wing," NASA CR 165749, March 1981.

[7]Rao, D. M., "Upper Vortex Flap—A Versatile Surface for Highly Swept Wings," International Council of the Aeronautical Sciences, ICAS 13th Congress Paper 82-6.7, Aug. 1982, pp. 1256–1266.

[8]Rao, D. M., "Vortical Flow Management for Improved Configuration Aerodynamics—Recent Experience," AGARD-CP-342, Paper 30, April 1983.

[9]Rao, D. M., "An Exploratory Study of Area-Efficient Vortex Flaps Concepts," *Journal of Aircraft*, Vol. 20, No. 12, 1983, pp. 1062–1067.

[10]Rao, D. M., and Johnson, T. D., "Investigation of Delta Wings Leading-Edge Devices," *Journal of Aircraft*, Vol. 18, No. 3, 1981, pp. 161–167.

[11]Frink, N. T., "Analytical Study of Vortex Flaps on Highly Swept Delta Wings," International Council of the Aeronautical Sciences, ICAS 13th Congress, Paper 82-6.7.2, Aug. 1982.

[12]Marchman, J. F., III, "The Aerodynamics of Inverted Leading-Edge Flaps on Delta Wings," AIAA Paper 81-0356, Jan. 1981.

[13]Marchman, J. F., III, "Effectiveness of Leading-Edge Vortex Flaps on 60 and 75 Degree Delta Wings," *Journal of Aircraft*, Vol. 18, No. 4, 1981, pp. 280–286.

[14]Schoonover, W. E., Jr., and Ohlson, W. E., "Wind-Tunnel Investigation of Vortex Flaps on a Highly Swept Interceptor Configuration," International Council of Aeronautical Sciences, ICAS 13th Congress, Paper 82-6.7.3, Aug. 1982.

[15]Hoffler, K. D., and Rao, D. M., "An Investigation of the Tabbed-Vortex Flap," *Journal of Aircraft*, Vol. 22, No. 6, 1985, pp. 490–497.

[16]Yip, L. P., and Murri, D. G., "Effects of Vortex Flaps on the Low Speed Aerodynamic Characteristics of an Arrow Wing," NASA TP 1914, Nov. 1981.

[17]Coe, P. L., Jr., and Weston, R. P., "Effects of Wing Leading-Edge Deflection on Low-Speed Aerodynamic Characteristics of a Low-Aspect-Ratio Highly Swept Arrow-Wing Configuration," NASA TP-1434, June 1979.

[18]Oh, S., and Tavella, D., "Analysis of a Delta Wing with Leading-Edge Flaps," *Journal of Aircraft*, Vol. 24, No. 6, 1987, pp. 353, 354.

[19]Oh, S., and Tavella, D., "Application of Vortex Cloud Method to Slender, Flapped Delta Wings," Joint Inst. for Aeronautics and Acoustics, Stanford Univ., JIAA TR-83, Stanford, CA, 1987.

Study of Dynamic Stall Using Real-Time Interferometry

L. W. Carr*
U.S. Army ATCOM and NASA Ames Research Center, Moffett Field, California 94035
M. S. Chandrasekhara†
Naval Postgraduate School, Monterey, California 93943
S. Ahmed‡
MCAT Institute, San Jose, California 95127
and
N. J. Brock§
Aerometrics, Sunnyvale, California 94086

Introduction

CONTROL and utilization, or alleviation, of the dynamic-stall-induced aerodynamic loads which appear on helicopter rotor blades, and on rapidly moving conventional aircraft wings or control surfaces, will require a much greater understanding of the character of the unsteady flowfield that occurs on these aerodynamic surfaces than is currently available. The complexity and rapidity of the flow development during dynamic stall as well as the large pressure gradients that form near the leading edge make quantitative measurement very challenging and difficult; the need for a clearer understanding of the effect of compressibility on the dynamic stall process further complicates this difficult task. However, traditional experimental techniques for analyzing aerodynamic flows are limited at compressible flow speeds; experimental data at these conditions on dynamically stalling airfoils has usually been restricted to surface measurements of pressure and skin friction. Interferograms showing the flow away from the surface of rapidly pitching airfoils have been obtained using holographic techniques.[1] However, the post-

Presented as Paper 91-0007 at the AIAA 29th Aerospace Sciences Meeting, Reno, NV, Jan., 7–10, 1991; received July 23, 1991; revision received June 15, 1993; accepted for publication July 21, 1993.

*Group Leader, Unsteady Viscous Flows, Aeroflightdynamics Directorate (ATCOM) and Fluid Mechanics Laboratory Branch (NASA), M/S 260-1. Member AIAA.

†Associate Director and Research Associate Professor, Department of Aeronautics and Astronautics, Navy-NASA Joint Institute of Aeronautics. Associate Fellow AIAA.

‡Currently Scientist, Experimental Aerodynamics Division, National Aeronautical Laboratory, Bangalore, India. Member AIAA.

§Currently Scientist, Metrolaser, 18006 Skypark Circle, Irvine, CA 92714.

processing associated with the creation of the requisite interferograms has usually limited the utility of holography to single interferograms of selected test conditions, with the interferograms created after the test has been completed. Real-time techniques such as Mach-Zehnder interferometry systems[2] require expensive optics, and need massive structure to reduce sensitivity to vibration. A new technique, based on the use of a vibration-insensitive real-time interferometry technique known as point diffraction interferometry (PDI), avoids these difficulties, while producing real-time interferograms, thus permitting on-line, detailed analysis and documentation of the dynamic stall process.

The point-diffraction interferometer technique used in the present test is based on the work of Smartt[3] as first applied to compressible flow by Bachalo and Houser,[4] combined with a self-aligning spot generation technique developed by Anderson and Milton.[5] In the present study, performed in the Compressible Dynamic Stall Facility[6] at the NASA Ames Research Center Fluid Mechanics Laboratory, the primary optics of an existing schlieren system were used, with a pulsed Nd:YAG laser replacing the conventional spark as the light source, and a specially created point diffractor replacing the usual knife edge. The laser light was expanded through a microscope objective to fill the schlieren mirror, transmitted through the test section, and refocused by another schlieren mirror. The exposed photographic plate used to create the point-diffraction spot was placed at the focus of this second mirror, and the laser was pulsed with enough energy to burn away the emulsion on the photographic plate in the vicinity of the focal point. This hole was created in situ by passing light through the test section at a no-flow condition, and was therefore precisely tailored to the application under investigation, automatically correcting for nonuniformities in the light source or optics (for further details concerning the implementation of the point-diffraction technique, see Ref. 7).

To obtain interferograms, the tunnel was turned on and the real-time interference fringes recorded on Polaroid film (ASA 3000) by pulsing the laser at the required angle of attack; the resultant interferograms were available for immediate viewing. This was of great value for analysis of the dynamic flowfield under investigation, since it permitted rapid review of the progress of the dynamic stall vortex, and detailed on-line study of the flowfield as it developed, since any phase of the cycle could be accessed directly.

Qualitative Analysis of Interferograms

Figure 1a presents a point-diffraction-interferometer image of the NACA 0012 airfoil at 0-deg angle of attack in steady flow at $M = 0.40$. The fringes seen in this photograph are constant-density contours, and therefore, constant-pressure contours (it is possible to compute the Mach number and corresponding inviscid pressure associated with each of these densities[8]). The stagnation point is characterized by the presence of circular fringes originating at the leading edge. The fringe pattern is symmetrical on both the upper and lower surfaces, indicating the flow is symmetric (appropriate for this airfoil, at 0-deg angle of attack). Since the fringe nearest to the leading edge encloses the stagnation point, correct Mach number values can be assigned to each of the fringes appearing on the airfoil. Some of the fringes generated at the leading-edge curve downstream, intersecting the airfoil downstream of the leading edge reflecting the decreasing velocity that exists on the airfoil surface downstream of the suction peak.

Figure 1b shows the fringe pattern of the NACA 0012 airfoil passing through 10.65-deg angle of attack, at $M = 0.40$, for a reduced frequency $k = \omega c/2U_\infty = 0.05$. The circular fringes now appear on the lower surface of the airfoil, reflecting the movement of the stagnation point due to the increase in angle of attack. The concentration of fringes near the leading edge shows the strong acceleration that occurs in this region. The fringes originating near the leading edge again curve back to the airfoil surface, indicating the presence of adverse pressure gradient on that part of the surface. The presence of the boundary layer can be seen by the abrupt turning of fringes in the downstream direction as they approach the airfoil surface.

Dynamic Stall as Shown by PDI

Figure 2 presents images of the flowfield for six angles during the upstroke for $M = 0.35$, $k = 0.05$. Figure 2a, taken at 10.65 deg, is similar to the image discussed above; Fig. 2b, taken at $\alpha = 12.11$ deg, shows similar characteristics, indicating that the flow is still attached. Figure 2c shows the character of the flow at $\alpha = 12.54$ deg; although the outer flowfield remains essentially unchanged, the fringes which rapidly curved back to the surface just downstream of the leading edge in Figs. 2a and 2b no longer do so. Instead, these are now displaced downstream, and show much less curvature

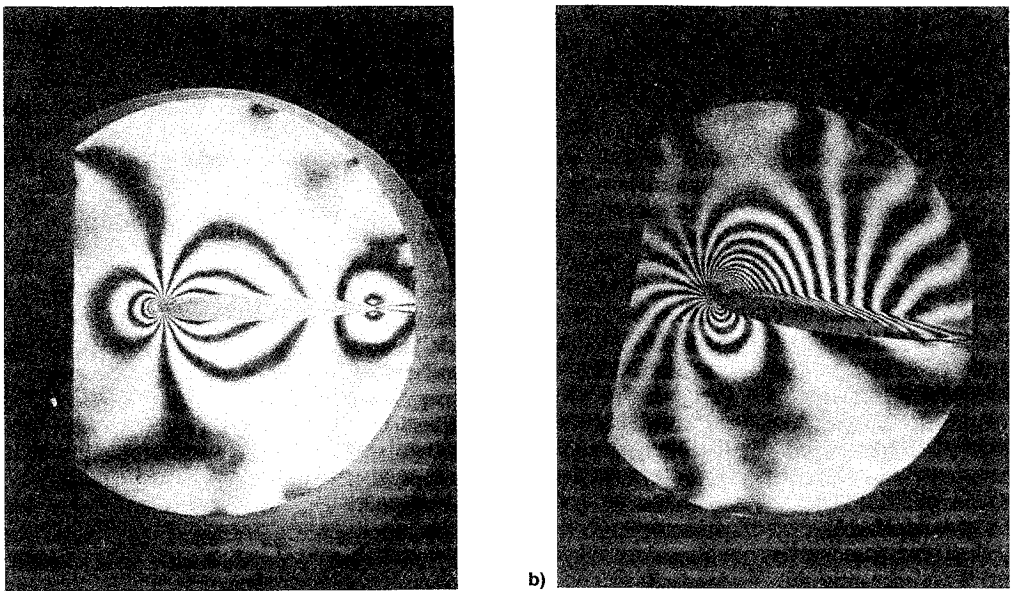

Fig. 1 Representative interferograms for NACA 0012 airfoil, $M = 0.40$: a) $\alpha = 0$ deg, $k = 0.0$ and b) $\alpha = 10.65$ deg, $k = 0.05$.

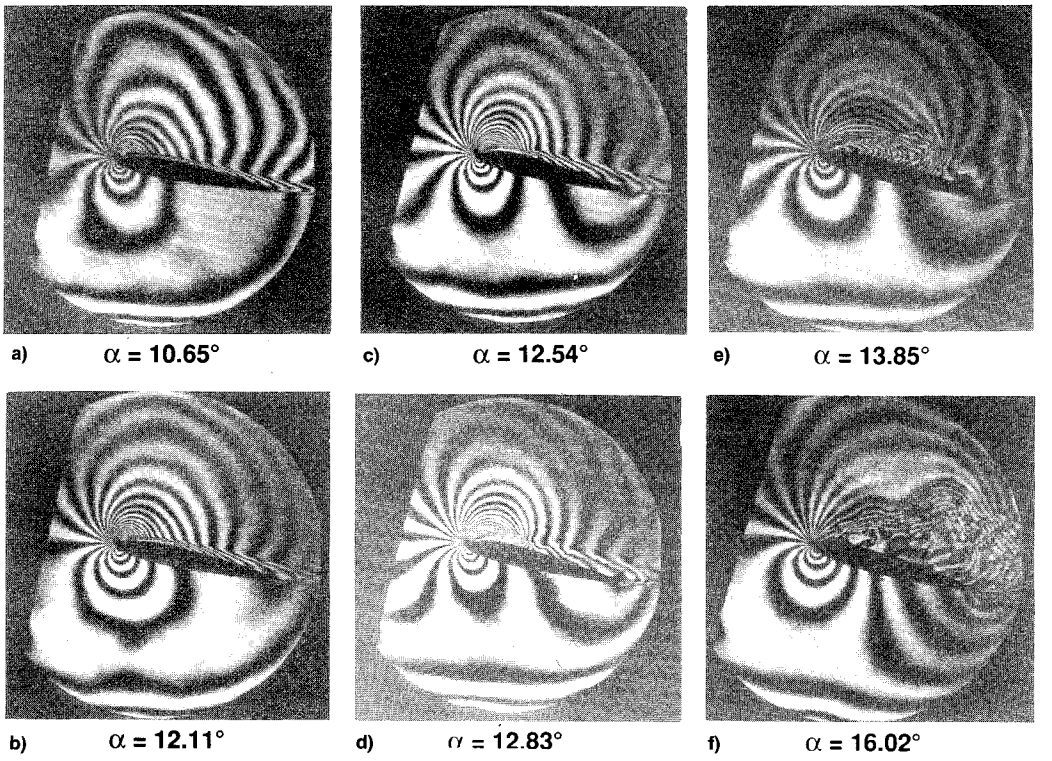

Fig. 2 Sequence of interferograms showing development of dynamic stall on an oscillating airfoil at selected angles of attack; $M = 0.35$, $k = 0.05$.

until they again come close to the surface, where they abruptly turn normal to the surface. This is the first indication that dynamic stall *delay* (the static stall angle for $M = 0.35$ is 11.6 deg) has ended, and that the dynamic stall process *itself* has begun. Figure 2d shows this flow for $\alpha = 12.83$ deg; here, the imprint of the dynamic stall vortex is more clearly delineated. The fringes near the leading edge terminate normal to the surface, and a few of them are curving against the direction of flow, showing the formation of a vortex-like structure. For this case, the outer flowfield is still attached. In fact, the outer flow fringes pass smoothly around the dynamic stall vortex, and blend into the boundary layer from 40% chord to the trailing edge.

At $\alpha = 13.85$ deg (Fig. 2e), the vortex has moved further down the airfoil, and has grown vertically. Although the interference fringes in the downstream part of the vortical region still show contours that might be expected from a classical vortex, the upstream part of the vortical region is much different from that which would be expected from such a vortex. Instead, all the fringes emanate from the leading edge, and enclose a fringe-free region above the airfoil surface. Since this region is vortical in nature, it is not clear that the fringes are still denoting constant velocity contours deep inside this region. It should be noted that the outer flowfield was not changed significantly (as evidenced by the unchanged pressure field delineated by the observed fringe pattern) until the dynamic stall induced flow reached the trailing edge of the airfoil (shown in Fig. 2f, $\alpha = 16.02$ deg). This is in agreement with the lift calculated from integration of instantaneous pressure transducer readings obtained on the surface during related dynamic stall tests,[9] which show the lift increasing until the dynamic stall vortex has left the trailing edge.

Conclusions

Real-time interferometry has now been demonstrated for analysis of unsteady compressible flow on dynamically stalling airfoils. In contrast to holographic interferometry, real-time techniques permit immediate review and evaluation of the resultant interferograms. This capability is a major value in analysis of dynamic flowfields such as those created by dynamic oscillation of airfoils, and dramatically improves the continuity of analysis of the aerodynamic events; this continuity is critical to improved understanding of dynamic stall.

The interferograms obtained in the present experiment suggest that the dynamic stall vortex produced by airfoil oscillation in the range of conditions studied does not immediately produce the symmetric imprint on the density field that would be expected from a classical vortex. Instead, these images imply that the dynamic stall develops as a region of strong gradients enclosing a region of low energy or weak structure, while still supporting the dynamically modified outer flow associated with the increase of lift that is typical of dynamic stall.

Acknowledgments

The project was supported by AFOSR-ISSA-89-0067 and AFOSR-MIPR-90-0012 (monitored by H. Helin and L. Sakell) with additional support from NAVAIR (T. Momiyama) and ARO MIPR-ARO-132-90 (T. L. Doligalski).

References

[1]Lee, G., Buell, D. A., Licursi, J. P., and Craig, J. E., "Laser Holographic Interferometry for an Unsteady Airfoil Undergoing Dynamic Stall," *AIAA Journal*, Vol. 22, No. 4, 1984, pp. 504–511.

[2]Jaeschke, M., Hiller, W. J., and Meier, G. E. A., "Acoustic Damping in a Gas Mixture with Suspended Submicroscopic Droplets," *Journal of Sound and Vibration*, Vol. 43, No. 3, 1975, pp. 467–481.

[3]Smartt, R. N., "Point-Diffraction Interferometry as a Diagnostic for Alignment," *Proceedings of the Meeting on Optical Alignment II*, Society of Photo-Optical Instrumentation Engineers, Vol. 483, 1984, pp. 78–83.

[4]Bachalo, W. D., and Houser, M. J., "Evaluation and Application of a New Interferometric Technique for Compressible Flow Research," NASA CR-177467, Oct. 1988.

[5]Anderson, R. C., and Milton, J. E., "A Large Aperture Inexpensive Interferometer for Routine Flow Measurements," *ICIASF'89 Record*, Inst. of Electrical and Electronics Engineers, Publ. 89-CH-2762-3, pp. 394–399.

[6]Carr, L. W., and Chandrasekhara, M. S., "Design and Development of a Compressible Dynamic Stall Facility," *Journal of Aircraft*, Vol. 29, No. 3, 1992, pp. 314–318.

[7]Brock, N. J., Chandrasekhara, M. S., and Carr, L. W., "A Real Time Interferometry System for Unsteady Flow Measurements," *ICIASF'91 Record*, Inst. of Electrical and Electronics Engineers, Publ. 91-CH-3038-8, pp. 423–430.

[8]Goldstein, R. J., "Optical Systems for Flow Measurement: Shadowgraph, Schlieren and Interferometric Techniques," *Fluid Mechanics Measurements*, Hemisphere, New York, 1983, pp. 377–422.

[9]Lorber, P. F., and Carta, F. O., "Airfoil Dynamic Stall at Constant Pitch Rate and High Reynolds Number," *Journal of Aircraft*, Vol. 25, No. 6, 1988, pp. 548–556.

Simple Equations for Helical Vortex Wakes

D. H. Wood*
University of Newcastle,
Callaghan, New South Wales 2308, Australia

Introduction

THIS Note is concerned with the equations describing the wake of a propeller, wind turbine, or helicopter rotor in hover or vertical flight. In all cases, the simplest possible vortex structure in the far-wake (well downstream of the blades) consists of N helical "tip" and "hub" vortices. N is the number of blades and the quotation marks indicate that these vortices may have been modified by vortex merger in the near-wake close to the blades. This structure leads to a straightforward equation for the axial velocity in the far-wake which is substituted into the conservation equations for mass, momentum, angular momentum, and energy. The resulting equations for the pitch of the tip vortex compare favorably to some measurements for propellers, but less favorably for hovering rotors. The energy equation contains the thermodynamic efficiency whose physical basis is well-founded. For reasons that are not entirely clear, it appears that the efficiency should also be included in the torque equation. If this is correct then the near-wake cannot be force-free.

Development of the Equations

From the analysis of the Biot-Savart law in Ref. 1, the average axial velocity in the far-wake of a propeller containing only tip and hub vortices is

$$U_\infty = 1 + N\Gamma/2\pi p_\infty \tag{1}$$

where Γ is the maximum bound circulation of each blade, and p_∞ is the pitch of the tip vortex in the far-wake. All lengths are normalized by the blade radius and all velocities by the freestream velocity U_0. Note that U_∞ is independent of the details of the hub vortex and that Eq. (1) applies to the irrotational flow that is assumed to fill the region between the tip and hub vortices. In other words, Eq. (1) takes no account of the wake of the blades. In deriving Eq. (1), the induced velocity has been averaged in the circumferential direction, but not radially. Nevertheless, as required by irrotationality, the average velocity is independent of radius in the far-wake, which is the situation assumed in the usual one-dimensional analysis that leads, e.g., to the Betz limit for wind turbines.

If there is no pressure difference across the wake, and the radius of the tip vortex is much greater than that of the hub vortex, then the axial momentum equation can be written in conventional form as

$$C_T = 2U_\infty(U_\infty - 1)R_\infty^2 \tag{2}$$

where C_T is the thrust coefficient, and R_∞ is the radius of the far-wake. A similar analysis gives the equations expressing conservation of energy and angular momentum. In forming the latter, the angular momentum Wr, where W is the circumferential velocity and r is the radius, is replaced by $N\Gamma/2\pi$. The equations are

$$\eta C_P = U_\infty(U_\infty^2 - 1)R_\infty^2 \tag{3}$$

$$= NU_\infty\Gamma R_\infty^2 J^{-1} \tag{4}$$

where C_P is the power coefficient, and J is the advance ratio. η is the thermodynamic efficiency, which is not to be confused with η_P, the conventional propulsive efficiency for a propeller. The relation between the two efficiencies is

$$\eta_P = 2\eta(1 + U_\infty)^{-1} \tag{5}$$

It is common in thermodynamic analyses to include η in the energy equation—Eq. (3)—to account for the irreversible conversion of mechanical into internal energy by the action of viscosity, but most "aerodynamic" analyses do not do so, see, e.g., Eq. (11) of Ramachandran et al.[2] The appearance of η in the angular momentum equation—Eq. (4)—is also unusual and requires careful justification. This will be attempted below.

Comparison with Experiment

If C_T and C_P are known, then Eqs. (1–4) contain five unknowns: U_∞, Γ, p_∞, R_∞, and η.

Knowledge of one of the five renders the equations solvable for the others, and so allows an assessment of the simple wake equations. The author knows of no wind turbine wake measurements for which this can be done, but there is sufficient detail in the four-bladed propeller data of Ref. 3 for a mean pitch angle of 27 deg. C_T and C_P were obtained from Figs. 8 and 9, respectively, and R_∞ from Fig. 5b, all from Ref. 3, allowing estimates to be made for U_∞, Γ, p_∞, and η. The pitch can then be compared to the experimental results in Fig. 5a, also from Ref. 3. Combining Eqs. (3) and (4) and using Eq. (1) gives

$$p_\infty = J(1 + U_\infty)/2\pi \tag{6}$$

This suggests that the pitch at the blades p_1 is given by

$$p_1 = J(1 + U_1)/2\pi \tag{7}$$

where conservation of mass gives the velocity at the blades as $U_1 = U_\infty R_\infty^2$. Equations (6) and (7) are shown in Fig. 1 to be a reasonable fit to the data. Generally, both are an improvement on the "light-loading" approximation $p = J/\pi$, see, e.g., Eqs. (1–3) of Hess and Valerazo.[4] Equation (7) crosses the J/π line because $U_1 < 1$ for the two highest values of J (and $U_1 \approx 1$ for the third). This physical impossibility may well be a consequence of the crudeness of the present

Received Dec. 11, 1992; revision received May 11, 1993; accepted for publication July 24, 1993.

*Associate Professor, Department of Mechanical Engineering.